

POA Investigation of FOS Dark Correction

P. Bristow, A. Alexov, F. Kerber & M. Rosa

November 2002 , 11 rev PB 12.11.2002 15:30

Abstract

*The dark flux correction step of the Faint Object Spectrograph calibration pipeline was investigated with the joint aims of applying a more physical model and improving the performance of the pipeline. After processing with the original **calfos** pipeline, dark calibration data shows a large scatter in count rates. We were able to reduce this scatter to some extent by scaling the correction according to the magnetic shell parameter. However, we were unable to find other parameterisations, having either an empirical or physical basis, which would reduce this scatter further. The distribution of the size and intensity of dark events, epoch dependency and the form of the diode mask were also investigated.*

Key words: *Data Reduction, Calibration, Space Telescope. Faint Object Spectrograph, Dark correction, dark particle flux, Data Archive*

1.Introduction

The FOS "darks" are defined as those counts accumulated in the absence of light shining through the entrance apertures - whether target or sky. The average dark count rates in orbit were of order 0.010 counts s^{-1} diode $^{-1}$ on FOS/RD and 0.007 counts s^{-1} diode $^{-1}$ on the FOS/BL side detector. The vast majority of these dark counts were due to fast particles generating Cerenkov light pulses in the entrance windows of the Digicon tubes. Compared to those events the average rate of 10^{-5} counts s^{-1} diode $^{-1}$ of electrons emitted thermally from the photo cathodes can be neglected for the present purpose.

The "Dark" correction step in the FOS pipeline is an attempt to subtract an appropriately scaled smooth distribution of "the average number of counts per pixel that would have been observed" during a given exposure. This step is carried out by default for all datasets except those obtained in IMAGE mode (see HST Data Handbook). The correction is made on a diode by diode basis. If a paired aperture was used and one of them had been specifically designated as "Sky", then a smoothed version of the observed "Sky" is subtracted from the "Object". Of course, the observed "Sky" includes a particle background as well.

However, if no contemporaneous background spectrum was obtained with the observation - the situation for nearly all FOS data, and the only situation which concerns us here - then scalable distributions (normalized counts vs diode maps) are used for FOS/RD and FOS/BL detector data respectively. The following analysis is restricted to FOS/BL except where explicitly noted.

Far more significant than the diode to diode dark count variation is the overall normalisation. This has been parameterised as a function of the spacecraft's geomagnetic latitude and longitude with empirical fits to the dark exposure data obtained (see eg. Rosenblatt et al. 92, Lyons et al. 92). This parameterisation is stored in the CCS8 table and is used to scale the diode map for the appropriate detector. The result is then stored in the .c7h file and subtracted from the raw data for further correction in the pipeline.

It was noticed early during the FOS on-orbit life that the above mentioned parameterisation left a considerable scatter in the observed dark count rate data, suggesting that there may be additional factors influencing the dark level (cf. Rosa 94) or that a model with geographic latitude dependency only might be too simple. In possession of the complete history of FOS Dark Calibration data, we investigate here a more physically motivated parameterisation and look for additional parameters which may allow us to estimate more accurately the dark background for a given exposure.

Section 2 introduces the calibration data used in our investigations and section 3 describes the principle methods of investigation. In section 4 we describe our findings regarding the distribution of dark features on the diodes and in section 5 we discuss the more important question of the normalisation of the dark correction as a function of a number of possible parameters. Section 6

explains a correction we made to a minor bug in the original *calfos* pipeline and section 7 presents our conclusions.

2.Data

There are some 2000 dark calibration datasets from all epochs of FOS's operational lifetime, of these only 130 had exposure times of more than 500 seconds. We used a sub-sample of 1560 datasets which have a common format of 23 groups by 512 diodes. As we were primarily interested in the normalisation the total counts from each group was of most interest to us. However, the shape of the counts vs diode distribution was also checked. Though a small change in form with time was noted, this was very small compared to the changes in overall normalisation and its effect upon real data would be virtually undetectable.

Besides the raw counts from the file itself additional parameters were gathered from several other sources. The OPUS database tables and dataset header files sufficed for most parameters. As noted in previous POA-FOS technical reports (eg Bristow et al. 2002), these sources are not always reliable. However, by running the datasets through *poa_calfos* we were able to obtain more accurate and reliable values regarding the timing of the exposures and the ephemeris and attitude of the spacecraft.

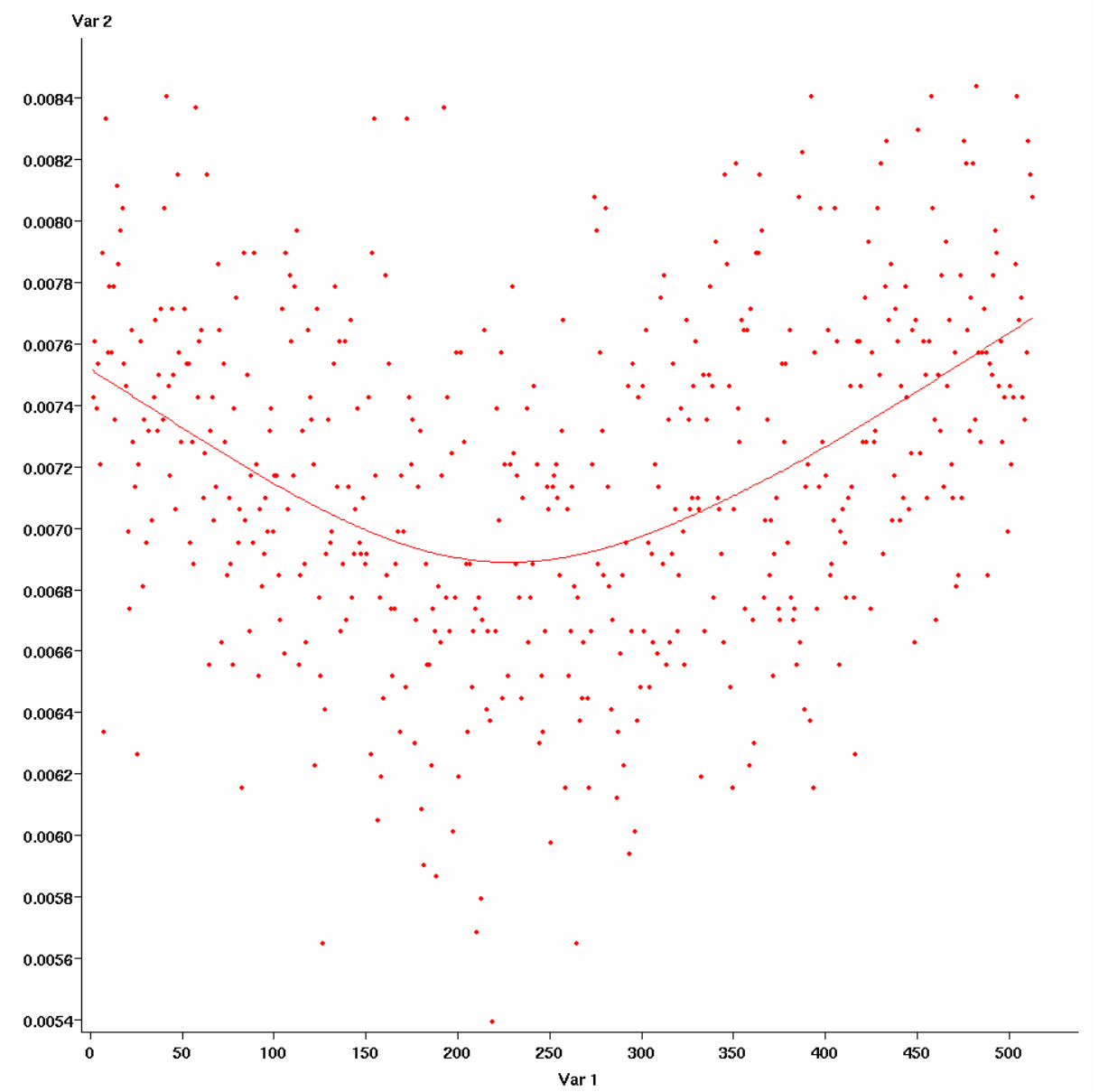
3.Analysis

Essentially the data under consideration consist of $1560 \times 23 \times 512$ (=18370560) integer results from the exposure of each diode which we may compare with physical parameters regarding the spacecraft (most obviously time and location). In principle obtaining statistics such as counts per diode, counts against time, counts against location etc. is straight forward, however a number of pitfalls had to be avoided:

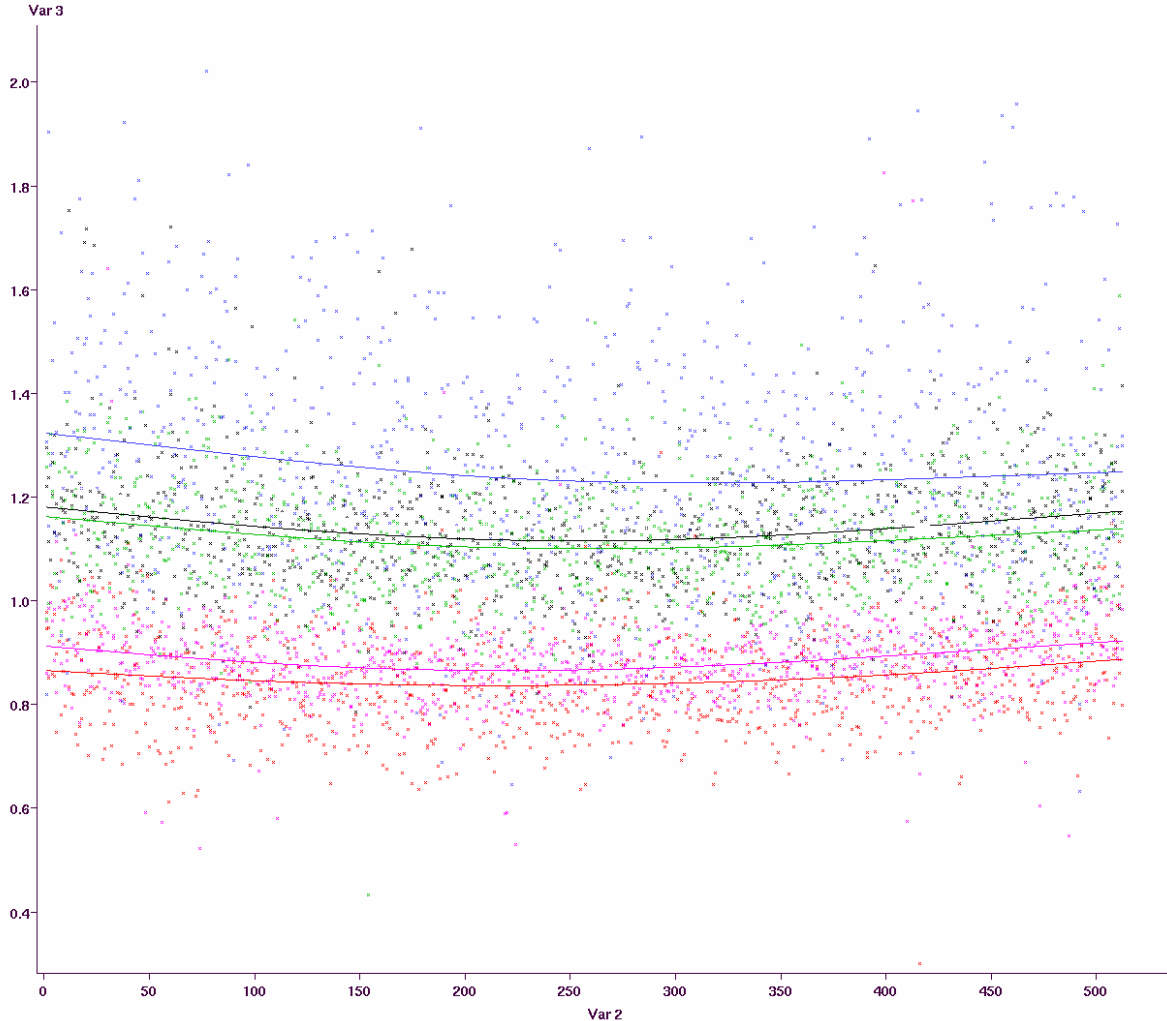
1. All of the analysis presented here is based on data obtained while the HST was far enough away from the South Atlantic Anomaly region to be unaffected.
2. Bad or noisy diodes were identified automatically and their contribution to the counts and the exposure time (both for the diode and the array) was not included in further analysis.
3. The time and position of each sub-exposure was different. From the values supplied in the header (start time for the first sub-exposure). Subsequent start times and locations were extrapolated. The sub-exposures were short enough that the change in location during the sub-exposure could be ignored and an average position was used.

4. Diode Statistics

The empirically derived FOS/BL diode dark rate map is confirmed when compared to data covering the FOS lifetime (Figure 1). Some small changes in shape are seen over time (Figure 2), but this change in shape is small compared to the change in normalisation. In fact the shape of the diode dark map can be seen to be a small effect indeed if the depth of the troughs on the smoothed diode response curves is compared to the normalisation.

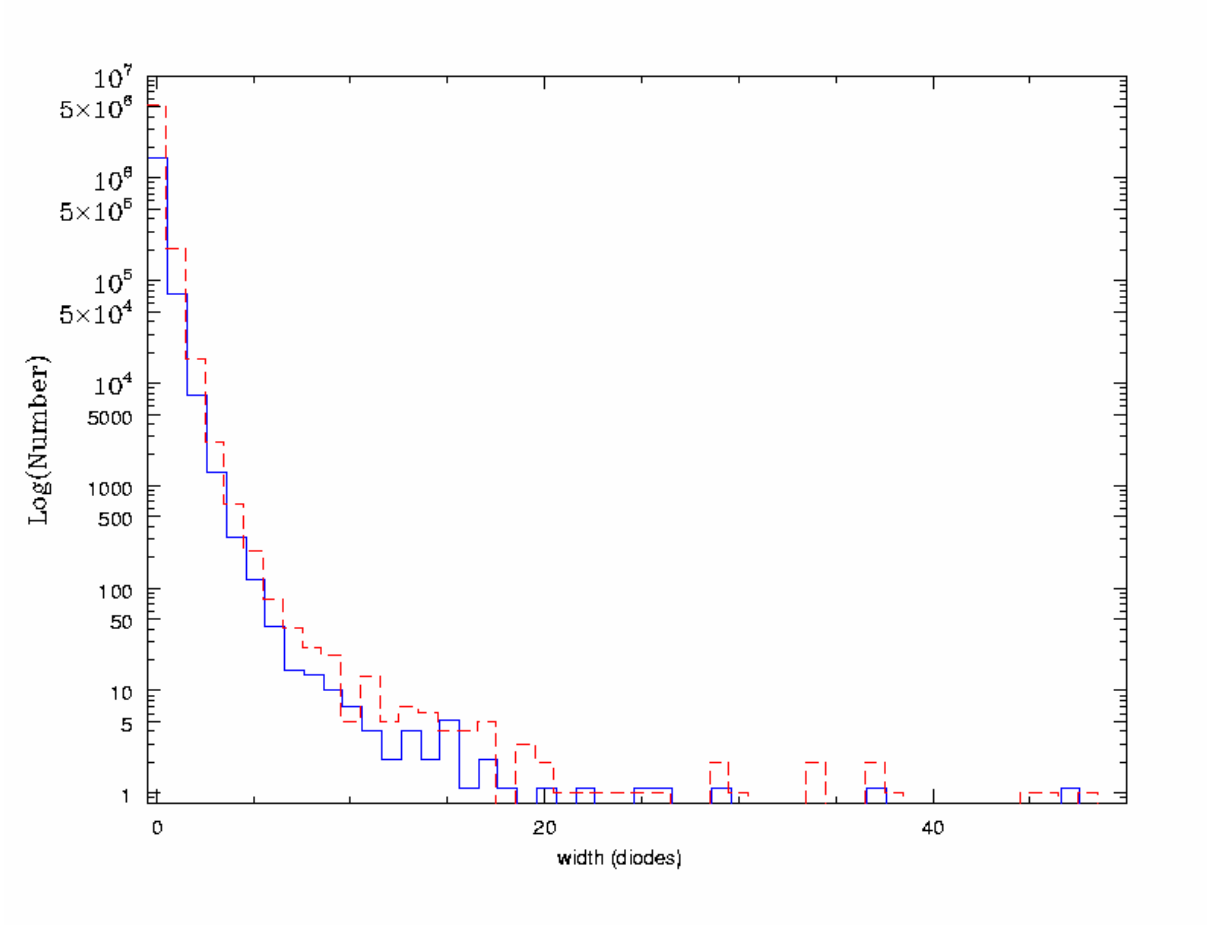


□ Figure 1 Distribution of dark counts across the BLUE detector diodes. The points are actual count rates for individual datasets whilst the line is a smoothed spline fit.

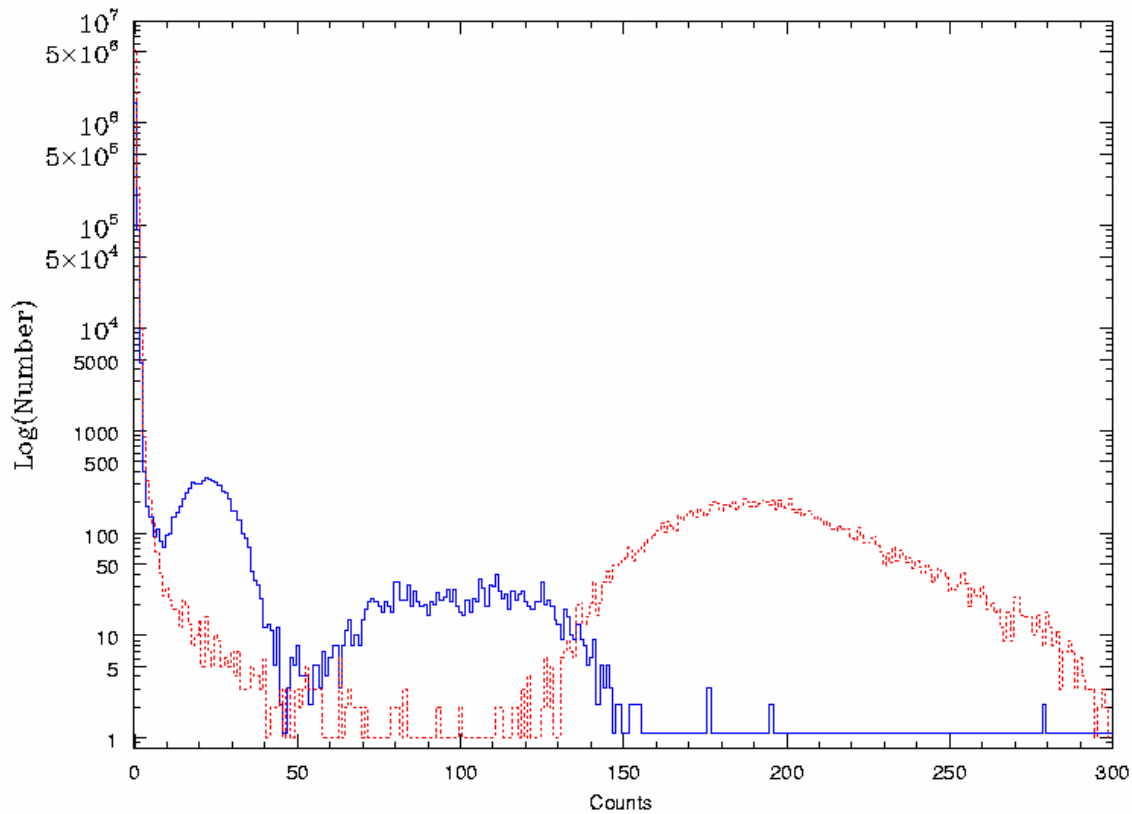


□ Figure 2: BLUE detector diode sensitivity at epochs throughout the FOS lifetime. The colours represent different epochs. The points are actual count rates for individual datasets whilst the lines are smoothed spline fits.

Furthermore statistics were compiled regarding the width and intensity of the dark count pulses, which are typically composed of signal in several adjacent diodes (Figures 3 and 4). Note the characteristic shape of the intensity distribution for the two detectors. The low intensity level feature in both detectors is likely due to thermal emission while the one peaking at very high intensities results from particles inducing Cerenkov light pulses in the faceplates. The fact that the thermal feature is seen at slightly higher intensities on the RED detector reflects the lower emission potential at the cathode. The differing position of the high intensity features stems from the different materials used in the faceplates. The distribution of widths (Figure 3) of the Cerenkov radiation induced counts emitted when high energy particles pass through the face plate of the detector. For some incident angles and points of impact this radiation will be spread over a range of pixels, for others it will be more intense (at the high end of the distribution) and effect less pixels. See Rosenblatt et al (1991) and Lyons (1992) for further discussion.



□ Figure 3: Distribution of widths of dark features on the FOS BLUE (solid) and RED (dashed) detectors.



□ Figure 4: Distribution of the intensity of dark features on the BLUE (solid) and RED (dotted) FOS detectors

5. Dependencies

Location in the Geomagnetic Field

As can be expected the clearest dependency of the counts is upon the spacecrafts orbital position, more specifically its location in the geomagnetic field. This dependency was already reflected in the calfos pipeline by a lookup table containing to an empirical scaling with geomagnetic longitude and latitude (CCS8 table). This simple scaling with coordinates in a dipole field provided a reasonable fit for most of the bulk of data. However, we were able to make a significant improvement by using a more physically motivated model.

Since the dark observed in FOS is due to charged particles (Cerenkov light), it is reasonable to try orbital dependencies that characterize the particle flux, rather than the magnetic field itself.

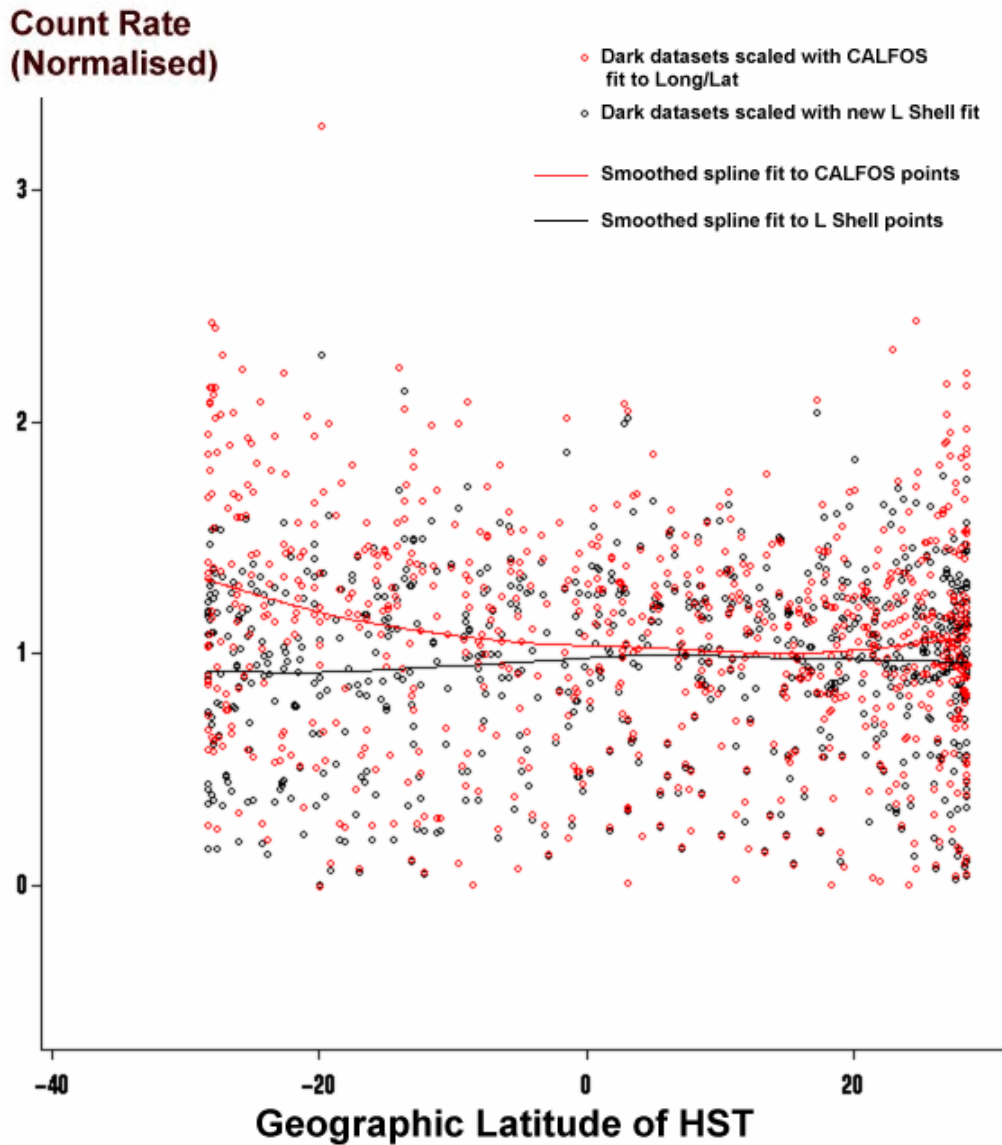
One such parameter that has been used extensively to interpret the particle flux data observed with other spacecraft is the so-called "magnetic shell parameter L" (C.-G. Faelthammar, p. 137). Citing from that reference: "In representing observed fluxes of trapped particles it is essential to take into account that their actual drift shells deviate from the simple shapes that apply in a pure dipole field." Using this shell parameter L and the magnetic field strength B one can organize the charged particle observations in the radiation belts in a BL coordinate system. The magnetic shell parameter L itself takes on the meaning of a length measured in units of earth radii, corresponding to the distance of equatorial crossing for a field line in case of a pure dipole field.

The functional form of L is approximately an inverse cosine square of a generalized geomagnetic latitude. We used the L-Shell parameter as defined and determined in the SHELLIG code segment from the implementation of the IGRF-Model (International Geomagnetic Reference Field), downloadable from the GSFC web server. Normalisation was then obtained from a comparison with the dark datasets. This semi-empirical approach gives an acceptable fit to most of the dark data but is less convincing at extremes of latitude.

To first order dark (particle) flux should simply be directly proportional to this parameter, so we made a linear fit and obtained:

$$N \text{ [counts/s]} = 0.0071228145 L_{\text{shell}} - 0.0022575311$$

Figure 5 shows a comparison between the calibration data corrected with the old POA calcos longitude/latitude parameterisation and the same data corrected with this new formula. Further investigation used data with this correction already applied.



□ Figure 5: Count rates from dark calibration datasets corrected with the CALFOS long/lat relation and the new POA L-Shell formula plotted against geographic latitude. The new L-Shell relation can be seen to give an improved correction at extremes of latitude. The calfos correction does not fully remove the dependence upon L—Shell. This is also seen for high latitudes.

Epoch and Solar Cycle

Next one might expect to find the particle flux to vary according to the solar cycle. The operational lifetime of the FOS spanned about two thirds of a complete cycle, starting from the maximum that occurred near launch. Variations over long time scales are indeed seen in the calibration data, however they are only very subtle and when compared to the solar cycle no correlation was found. Further attempts to find a correlation with various sources of measured particle flux during this epoch also failed. Had such a correlation been found, it would have given credence to the notion that the subtle variations over time seen in the calibration data were real. In the absence of a correlation we decided that the subtle epoch dependence seen was unconvincing and elected not to introduce this as an additional correction in *poa_calfos*.

Day/Night

Dark count variations over smaller time scales may also be expected (see Rosa 1994). Indeed this may account for some of the scatter seen in the calibration data. A problem here is that calibration data, particularly darks, tend to be obtained during the bright part of the orbit, while real data is obtained during the dark part. This selection effect could lead to a systematic offset between the correction derived and that required. Rosa (1994) was able to show this by using data from the first fifty diodes from G130H BLUE and G190H RED science exposures. These diodes effectively record background light in these modes as they are cut off from the exposure due to absorption in the faceplates.

In order to investigate this further it was necessary to know, for all of the calibration exposures considered, the pointing of the telescope relative to the horizon and relative to the sun. As we have reported elsewhere (eg. Bristow et al. 2001), the pointing information in the dataset headers is unreliable and therefore not useful for investigations such as these.

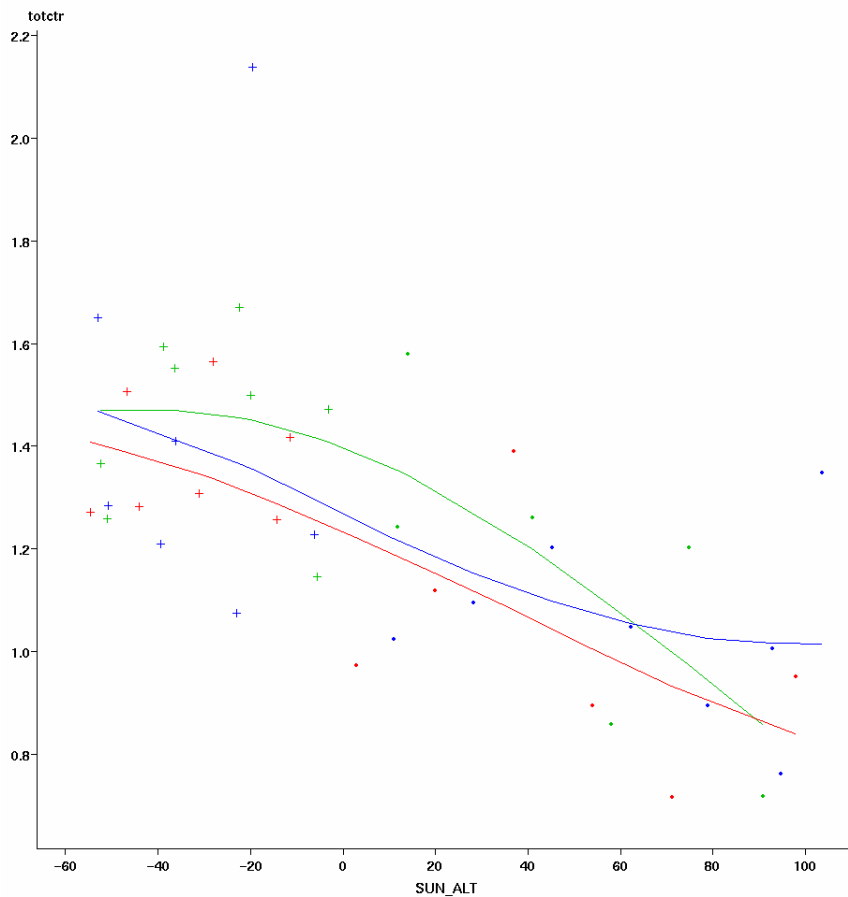
According to the HST Keyword Dictionary the SUNANGLE is the "angle between sun and V1 axis (deg)":

Computed from the spherical trigonometry formula:

$$\begin{aligned} \cos(\text{SUNANGLE}) = & \sin(\text{DECLSUN}) * \sin(\text{DECLNV1}) + \\ & \cos(\text{DECLSUN}) * \cos(\text{DECLNV1}) * \cos(\text{RTASSUN} - \text{RTASSUN1}) \end{aligned}$$

However it is clear that SUNANGLE values that appear in the headers of dark calibration observations were just calculated for constant values of DECLNV1 and RTASCNV1. So we had to obtain the V1 vector from processing the data first with *poa_calfos* processed data, after which we were able to calculate a correct value for the SUNANGLE.

Plotting dark counts (already corrected for the L-shell dependence) against SUNANGLE for all of the calibration data still showed no correlation. Restricting the comparison to data for which the sun was above the horizon, did not help (neither did the opposite restriction).



□ Figure 6: Dark count rate against SUN_ALT. The three colours denote groups having distinct SUNANGLE values. The points are actual count rates; the lines represent smoothed spline fits.

On the other hand, examining data from within a very short time window did show the kind of dependence expected. Figure 6 shows an example. Here we have "zoomed in" (in time) on three consecutive groups of calibration data. The three groups fall into three different, non-overlapping, SUNANGLE ranges, indicated by the three colours. About half of the observations in each group were obtained with SUN_ALT less than zero, these are indicated by the Xs (dots for SUN_ALT more than zero). The plot shows the dark counts against SUN_ALT with smoothed spline fits to each group. The trend is similar, though the normalisation varies by around ten percent. Fits to just the SUN_ALT less than zero data are much flatter, while the SUN_ALT dependence is stronger for positive values.

Whilst there is still considerable scatter, there is a clear trend here. Unfortunately this is washed out on longer time scales for a number of reasons. Firstly the behaviour is different in the regimes for which SUN_ALT is more than versus less than zero. Secondly, although similar trends are found by zooming in on other groups of exposures, the gradient of the SUN_ALT versus dark counts relationship changes gradually with time. Thirdly the normalisation changes in a more erratic fashion. Although this relationship seems to be real, it is only second order and there is no

obvious physical model that would explain the variation in gradient and normalisation.

Finally, the dark counts could be more sensitive to other parameters. We checked for correlation against many other header keyword and engineering parameters including:

MIDTIM
INTS
YBASE
NPAT
NREAD
MAXCLK
NOISELM
MOONANGL
YHVCUR
YHVTMP
YHVVL
YPMFATMP
YPMFBTMP
RA_SUN
DEC_SUN
Month of observation

and in addition against those extra parameters generated by the IGRF magnetic model code and the NORAD ephemeris code which are part of the *poa_calfos* pipeline. No clear dependencies were found.

We conclude at this point that the low statistical significance of the total counts collected during an individual dark exposure combine with the fluctuations, seasonal and secular variations that are known to exist in the particle flux density in such a way as to veil such dependencies. The FOS was not designed as an instrument to study the particle belts.

As a result of the above findings, the only parameterisation implemented was the L-Shell parameterisation (which replaced the previous latitude parameterisation). The others were considered to show a correlation to the calibration data which was either too weak or too difficult to model in a physical way. Last but not least the uncertainties in the normalization of the "dark" are significant only for the very faintest of all targets observed with FOS.

6. Bug Fix

When implementing the new L-Shell parameterisation we noticed an error in the way that the dark correction was made to ACCUMed data in the original *calfos* software. ACCUM was the most commonly used mode. Spectra were read out at 4 minute intervals and the accumulated sum after each read was recorded in consecutive groups on the standard output data files, i.e. each

consecutive spectrum was made up of all previous intervals of data in an ACCUM observation. The dark scaling, however, was appropriate to each spectrum individually and could vary considerably during an ACCUM observation as the spacecraft traversed a range of L-Shell (or latitude).

The original calfos pipeline applied the dark correction to the groups *without* “deaccuming” them. If this is done then the scale factor itself should be “accumed” (we needn’t worry about accumulating the whole dark diode mask as its shape is constant). We implemented the following simple algorithm to accum the scale factor:

Let the scale factors for the groups (deaccumed) be S_1 to S_n and the scaling factors for the accumulated groups be S'_1 to S'_n . Then;

$$S'_1 = S_1$$

and

$$S'_n = S_n + (S_{n-1})(n-1)/n$$

For ACCUM observations spanning a large range of L-shell this corrective algorithm could change the dark scale factor by as much as 30%.

The dark correction applied is written, for each group, (as a scaled diode map) to the *.c7h file. As this file accompanies the (eventually) deaccumulated group data it was, correct in the original calfos implementation, in that the *.c7h file would contain the dark correction that should have been applied to each group (but not that which was). Ironically, our correction put the accumulated dark corrections into the *.c7h files. This was easily corrected by making a separate call to the output routine with the diode map scaled by S_n and not S'_n .

7. Conclusions

We investigated a number of physically meaningful correlations between dark calibration data and parameters available from the dataset headers, the archive and engineering data. On the whole the results were disappointing. We were able to replace the existing latitude/longitude scaling with a more physically motivated model which fits the data somewhat better. However the remaining scatter is still large and the other correlations which we found were not able to reduce this significantly. There is clear evidence in the data of a dependence upon the spacecrafts pointing relative to the sun and position relative to the Earth’s shadow. However, this insight was limited by the available data (not just the existing datasets but also the reliability of header and archive content). In addition we made an algorithmic correction to the processing of data taken in ACCUM mode.

References

Bristow, P. D., Alexov, A., Kerber, F. & Rosa, M. R., 2001. **POA/FOS-2002-02**

R. W. Lyons, W. Baity, E. A. Beaver, R. D. Cohen, V. T. Junkkarinen, J. B. Linsky, E. I. Rosenblatt, 1992. **FOS ISR 080**

Rosa, M. R., 1994. in *"Calibrating Space Telescope"*, C. Blade and S. Osmer (eds), p190, **"Background Signals in FOS Data"**

E. I. Rosenblatt, W. A. Baity, E. A. Beaver, R. D. Cohen, V. T. Junkkarinen, J. B. Linsky, and R. Lyons, 1992. **FOS ISR 071**

Rosenblatt, E. I., Beaver, E. A., Cohen, R. D., Linsky, J. B., Lyons, R. W. 1991 **SPIE.1449...72R**